CrossMark

ORIGINAL PAPER

Design and preparation of a cellulose-based adsorbent modified by imidazolium ionic liquid functional groups and their studies on anionic dye adsorption

Su-Feng Zhang · Miao-Xiu Yang · Li-Wei Qian · Chen Hou ·
Rui-Hua Tang · Jin-Fan Yang · Xue-Chuan Wang

Abstract Adsorption of dyes via strong interactions between modified cellulose paper and dyes is an economical, effective, and sustainable method for treating wastewater. In this work, using multiple interactions with dye molecules, an imidazolium ionic liquid modified cellulose adsorbent (CCP-Im) was prepared and used to treat anionic dye wastewater effectively. Zeta potential tests and Gaussian simulations revealed the strong interactions between CCP-Im and anionic dye molecules. Under optimum adsorption conditions, CCP-Im has good adsorption capacity for anionic dyes, and the maximum adsorption capacities of xylenol orange and Congo red could reach 1169 and 563 mg g^{-1}, which were 3.1 and 3.5 times, respectively, higher than the values of the original cellulose paper. The Freundlich and Scatchard models for isothermal study demonstrated the adsorption process of CCP-Im toward anionic dyes occurred on a heterogeneous surface via multilayer sorption, and the kinetics revealed that a Pseudo-second-order model described the adsorption process well, indicating the adsorption was controlled by the mechanism of chemical adsorption. Therefore, preparation of this bioadsorbent would be useful for environmental protection and development of sustainable resources.

Keywords Cellulose · Dye · Adsorption · Imidazole · Ionic liquid

S.-F. Zhang (✉) · M.-X. Yang · L.-W. Qian (✉) ·
C. Hou · R.-H. Tang · J.-F. Yang · X.-C. Wang
Shaanxi Provincial Key Laboratory of Papermaking
Technology and Specialty Paper Development, Key
Laboratory of Paper Based Functional Materials of China
National Light Industry, National Demonstration Center
for Experimental Light Chemistry Engineering Education,
Shaanxi University of Science and Technology,
Xian 710021, China
e-mail: sufengzhang@126.com

L.-W. Qian
e-mail: qianliwei@mail.nwpu.edu.cn

L.-W. Qian · C. Hou · J.-F. Yang
Key Laboratory of Pulp and Paper Science & Technology
of Ministry of Education/Shandong Province, Qilu
University of Technology, Jinan 250353, China

Introduction

Industries and human activities discharge large quantities of pollutants that contain organic dyes, which can have a very negative environmental impact because they are toxic, nonbiodegradable, and have mutagenic effects on human health and marine organisms. Congo red (CR) and xylenol orange (XO) are the most commonly used dyes for printing and dyeing textiles and have proven to cause a variety of carcinogenic, teratogenic, and mutagenic diseases in

humans (Zhu et al. 2016). Therefore, it has become urgent to solve the problem of treating wastewater that contains these dyes.

In the process of removing dye from wastewaters, many treatment methods have been developed, including electrolysis (Umukoro et al. 2017), ultrafiltration (Lin et al. 2016), chemical flocculation (Han et al. 2016), chemical oxidation/reduction (Buthiyappan et al. 2016) and adsorption (Liu et al. 2018a, b). Among these methods, adsorption is considered to be a competitive method for treating dyestuffs in wastewater because of its economic feasibility, high efficiency, and operational simplicity. Activated carbon is a renewable and sustainable resource and is the most commonly used adsorbent for removing contaminants from air and wastewater because it has a high removal efficiency and does not produce harmful by-products (Maneerung et al. 2016). However, the higher production cost of activated carbon limits its further development and application. Thus, developing an inexpensive, efficient, and sustainable absorbent that can be used instead of activated carbon to remove dyes would have great prospects.

Cellulose is widely considered to be an inexhaustible and sustainable raw material (Trache et al. 2017). Paper is one of the earliest prepared cellulose materials and is expected to be a very promising adsorbent for replacing activated carbon because of its low cost and mature preparation process. However, hydrogen bonding interactions between the hydroxyl groups of cellulose-based paper and dye molecules are susceptible to water molecules in the aqueous phase and result in a lower adsorption capacity (Hokkanen et al. 2016). Grafting functional groups via electrostatic forces or π–π stacking on the surface of cellulose can solve this problem to a certain extent. Liu reported a nanofibrillated cellulose/chitosan composite modified with ethylenediamine to remove the anionic dye, new coccine (Liu et al. 2016), and the prepared material had an adsorption capacity of 103 mg g^{-1} as a result of strong electrostatic interactions. Xiao et al. (Xiao et al. 2016) demonstrated using L-cysteine reduced graphene oxide to remove anionic and cationic dyes, and the results showed that the π–π interactions between graphene and organic dyes with conjugated aromatic structure play a key role in the efficient removal of contaminates from the aqueous phase.

Furthermore, some available research has demonstrated that wastewater can be efficiently treated using multiple interactions between functionalized adsorbent and dye molecules. Veerakumar et al. (Veerakumar et al. 2017) synthesized 2D graphene oxide nanosheets that showed an adsorption capacity of 217 mg g^{-1} for eosin yellow, and this was attributed to complex driving forces, including hydrogen bonding, π–π conjugation, and electrostatic interactions. Qiu et al. (Qiu et al. 2009) used the synergistic effect of electrostatic forces and π–π stacking between straw-based biochar and dyes to obtain a good adsorption capacity of 313 mg g^{-1} on reactive brilliant blue.

Based on the above strategy, studying the use of imidazolium ionic liquid (IM-IL) functional groups to modify the adsorption performance of substrates has drawn worldwide attention. IM-IL is a functional material that has a cationic imidazole group and anionic free halogen or other anionic organic group. Because of the strong interactions with guest molecules via electrostatic forces, π–π conjugation, and hydrogen bonding (Qian et al. 2017; Mi et al. 2013), IM-IL modified materials have excellent adsorption performance for treating dyes in wastewater. Song proposed novel IM-IL-based hyperbranched polymers (Song et al. 2016), in which imidazole cation groups generate multiple interactions with dyes and result in an extremely superior adsorption capacity of 1993 mg L^{-1} for CR. However, there are still few studies regarding the modification of cellulose with IM-IL functional groups to treat dyes in wastewater.

In this work, a cotton cellulose-based paper (CCP) was selected as the substrate, and IM-IL groups were selected and used to modify CCP via esterification and alkylation reaction. The obtained modified bioadsorbent was characterized using Fourier transform infrared spectroscopy (FT-IR), X-ray photoelectron spectroscopy (XPS), and scanning electron microscopy (SEM). In addition, Zeta potential tests and molecular simulation calculations were carried out to analyze the interactions between IM-IL groups and dye molecules. Furthermore, the adsorption performances of the anionic dyes Congo red and xylenol orange were evaluated using adsorption experiments, and the adsorption behavior of each was investigated using adsorption isotherms, kinetics, and thermodynamics in the study.

Experimental

Materials

2-Bromopropionic acid (2-BPA, 98%) and 1-methylimidazole (99%) were analytical grade and obtained from Shanghai McLean Biochemical Technology Co., Ltd. (Shanghai City, China); para-toluenesulfonic acid (p-TSA) was analytical grade and obtained from Sinopharm Chemical Reagent Co., Ltd. (Shanghai City, China); Congo red (CR, IND), methylene blue (MB, IND), dimethyl yellow (DY, IND), and xylenol orange (XO, IND) were analytical grade and obtained from Tianjin Kemiou Chemical Reagent Co., Ltd. (Tianjin City, China). CCP (Ø 22 cm) had a basis weight of ca. 255 g m^{-2} and was obtained using refined cotton pulp from Tianjin Zhongchao Paper Co., Ltd. Other reagents were analytical grade and used without further purification.

Characterizations

FT-IR spectra were recorded on a Bruker VERTEX 70 spectrometer with ATR technique. SEM images were recorded using a TESCAN VEGA 3 Easy Probe. XPS was performed on a KRATOS AXIS Supra spectrometer for surface analysis with a monochromatized Al-Kα source (hv = 1486.6 eV) during analysis. The full spectra (0–1200 eV) were obtained at a constant pass energy of 40 eV. The Zeta potential of each sample in water was characterized using a Germany Mutek SZP-06 Zeta potential analyzer. The concentration of the dye solution was determined using a UV-2550 UV–Vis spectrophotometer (Shimadzu Co., Ltd.).

Synthesis of cellulose bromopropionate esters (CBE)

First, the reactant 2-BPA (17.6 g) and the catalyst p-TSA (0.14 g) were successively dissolved in 80 mL of toluene, and then the CCP (2.0 g) was immersed into the reaction system. The mixture was heated to reflux under Dean-Stark conditions (Song et al. 2016; Watson et al. 2017) in an oil bath at 130 °C, and after reacting for 7 h, it was cooled to room temperature. Then the mixture was washed with ethanol, 4% aqueous sodium carbonate solution, and deionized water. The product was dried at 30 °C to obtain cellulose bromopropionate esters (CBE).

Synthesis of ionic liquid modified cellulose products (CCP-Im)

A mixture of CBE (1.4 g) and 1-methylimidazole (16.4 g) in 60 mL of ethanol was stirred for 24 h at 70 °C to synthesize CCP-Im (Liu et al. 2017). The crude product was then washed with ethanol and deionized water and dried at 30 °C to obtain CCP-Im.

Computer simulation

To study the interactions between dye molecules and CCP-Im, density functional theory (DFT) calculations using the B3LYP functional with the 6-31G (d) basis set were carried out in this work. All of the DFT calculations were performed using the Gaussian 09 program. Similar DFT methodology has been successfully employed to study these interactions (Qian et al. 2017; He et al. 2015). According to a previous report (Guan et al. 2015), CCP-Im can be simplified as Compound **1** (as shown in Fig. S1), and this is the main factor that interacts with dyes. The binding energies (ΔE) between dye molecules and CCP-Im were evaluated using Eq. 1

$$\Delta E = E(\text{complex}) - E(\text{Compound } \mathbf{1}) - E(\text{dye}) \tag{1}$$

where E (Compound **1**), E (dye), and E (complex) were the potential energies of Compound **1**, the dye molecule, and their complex, respectively.

Adsorption experiments

Binding experiments were carried out to verify the adsorption performance of CCP-Im toward the dyes. A certain amount of CCP-Im was immersed completely to 10 mL of dye solution at a specific concentration without other operations. After the adsorption experiments, the concentrations of dyes in the remaining solution were analyzed using UV–vis spectrophotometry. The adsorption capacity (Q) was determined from Eq. 2 (Mir et al. 2018)

$$Q = \frac{(C_0 - C_t)V}{m} \tag{2}$$

where C_0 (mg g^{-1}) is the initial concentration of the dye, C_t (mg g^{-1}) is the concentration of the dye after a certain period of adsorption time, V (L) is the volume of the used dye solution, and m (g) is the weight of adsorbent.

Optimization of adsorption conditions To optimize the adsorption conditions and evaluate the adsorption capacity, different adsorbent dosages, values of pH, contact time, and initial concentrations of dyes were used to control variables of the procedure. All batch adsorption experiments were carried out at a fixed temperature and prescribed amounts of adsorbent were added to samples of 10 mL of dye solution that had a defined concentration (Góes et al. 2016). After the adsorption experiments, the dye solution was obtained, and the concentrations of dyes in the remaining solution were measured using UV–vis spectrophotometry. Also, the optimum conditions for adsorption were evaluated to determine the maximum adsorption capacity.

CCP was also subjected to the dye adsorption experiment under the same conditions to compare the adsorption capacity of CCP-Im and CCP toward dyes. Also, the impact factor (IF) was used to evaluate the increase in the adsorption capacity, and IF was calculated using Eq. 3

$$IF = \frac{Q_{CCP-Im}}{Q_{CCP}} \tag{3}$$

where Q_{CCP-Im} and Q_{CCP} are the adsorption capacities of CCP-Im and CCP, respectively.

Selective adsorption To evaluate the selective adsorption capacity of CCP-Im toward dyes (Fu et al. 2016; Yao et al. 2017), 0.05 g of CCP-Im was added to a 6 mL solution mixture that contained CR and MB with a concentration of 5 mg L^{-1}. After the adsorption reached saturation, the remaining solutions were measured using UV–vis spectrophotometry at 664 and 497 nm for MB and CR, respectively.

Recycling studies The recycling stability of the adsorbent was evaluated using a procedure of repeated CR adsorption–desorption (Melo et al. 2018). First, for the adsorption cycles, solutions of 2000 mg g^{-1} CR were static with the CCP-Im adsorbent (5 g L^{-1}) at 25 °C for 24 h. Then, the CCP-Im material that adsorbed the CR species was subjected to a desorption process in 50 mL of HCl aqueous solution (0.5 mol L^{-1}) at 25 °C for 30 min to remove CR (Peng et al.

2018). Recovered CCP-Im was then subjected to the next adsorption cycle of the experiment under the same conditions. After the adsorption experiments, the remaining solutions were measured using UV–vis spectrophotometry to determine the adsorption capacity (Q_n). The relative ratio of the adsorption capacity among each cycle were calculated by Q_n/Q_0, where n was the recycling number.

Results and discussion

In this work, a novel IL functional group modified bioadsorbent was designed and prepared via simple esterification and alkylation reactions with cellulose, as shown in Fig. 1. Due to the strong electrostatic forces, hydrogen bonding, and π–π stacking between imidazolium cation and anionic dyes, the prepared bioadsorbent was expected to exhibit good adsorption capacity and selectivity.

Chemical structure and elements analysis

FT-IR analysis The chemical structures of the cellulose paper before and after adsorption were analyzed using FT-IR (Fig. 2). First, the spectrum of CCP shows typical absorption bands of the cellulose backbone at 1104, 2915, and 3340 cm^{-1}, which are attributed to C–O–C, C-H, and O–H bonds, respectively. Compared to the FT-IR spectrum of CCP, the FT-IR spectrum of CBE (Chen et al. 2017) reveals a new band at 1721 cm^{-1}, which corresponds to the stretching mode of the carbonyl group (C=O) of the newly formed ester linkage between CCP and 2-BPA. In addition, the FT-IR spectrum of CCP-Im shows some new bands at 1207, 1454, and 1637 cm^{-1}, and these are typical absorption bands for C–N, C=C, and C=N, respectively, of the imidazole group (Karatzos et al. 2011; Boakye et al. 2017). This suggests that the IM-IL structure was successfully grafted onto the cellulose backbone.

XPS analysis XPS analysis of both the original and functionalized cellulose provides important information regarding changes to the surface elemental composition that occur when the imidazole group is immobilized. As shown in Fig. 3a, the spectrum of CCP only shows peaks for carbon and oxygen atoms at 285.0 and 531.8 eV, respectively. After esterification with 2-BPA, the survey spectrum of the prepared CBE
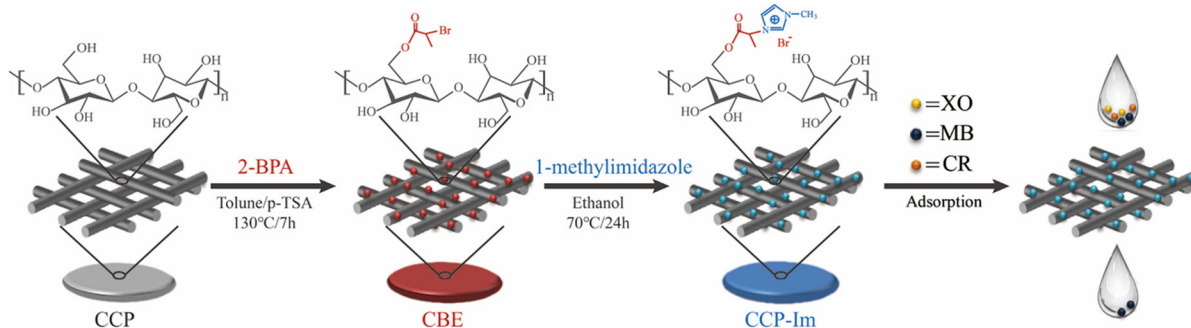
Fig. 1 Schematic illustration of the synthesis of the CCP-Im adsorbent and its adsorption performance for dyes
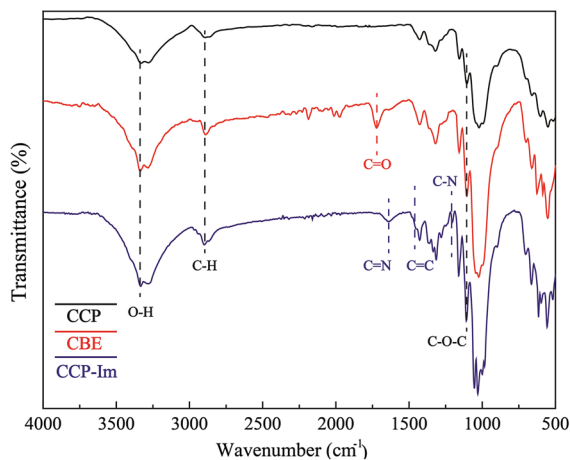

Fig. 2 FT-IR spectra of CCP, CBE, and CCP-Im

shows a new peak at 69.0 eV; this is attributed to bromine atoms, confirming that the esterification reaction was successful (Fig. 3b) (Qian et al. 2017). Compared to the spectra of CCP and CBE, the survey spectrum of CCP-Im shows a new peak at 399.7 eV, which is attributed to the nitrogen atom of the imidazole functional group. The presence of imidazole

further confirms that the IM-IL structure was successfully grafted onto cellulose (Fig. 3c).

Surface morphology analysis

SEM was used to investigate the effects of the esterification and alkylation reactions on the morphologies and microstructures of the cellulose fibers and paper (Li et al. 2015). As shown in Fig. 4a, the SEM images at low magnification show that the fibers of the original CCP exhibited an expected ribbon-like structure, in which individual fibers could easily be identified and the surface of the fiber was intact and smooth. After the esterification and alkylation reactions, a low-magnification image of CCP-Im (Fig. 4c) shows that the structural integrity and the original interwoven state of the fiber were basically retained. However, further examination of SEM images at high magnification reveal that the surfaces of the modified cellulose fibers were rougher than the base paper, and this also provides evidence that the IM-IL structure was grafted onto the cellulosic backbone.
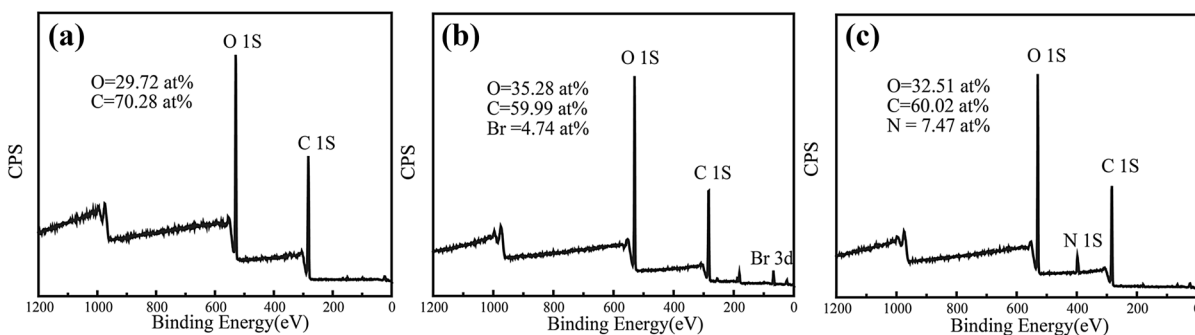
**Fig. 3** Survey spectra of **a** CCP, **b** CBE, and **c** CCP-Im (Elemental content is provided in each panel)
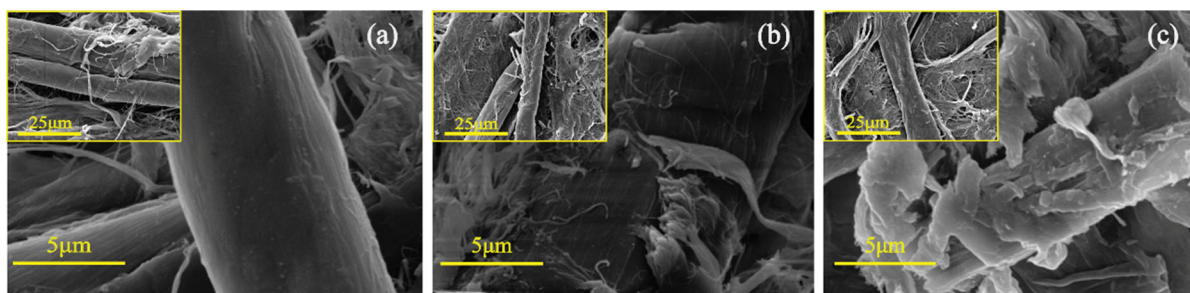
Fig. 4 SEM images of **a** CCP, CBE, and **c** CCP-Im

Zeta potential analysis

Because grafting IM-IL functional groups may directly affect the charge on the surface of cellulosic material, Zeta potentials were measured in this work (Song et al. 2017). As shown in Fig. S2, when the pH was 7, compared to the value of the Zeta potential of CCP, that of CBE was significantly increased from − 39.9 to − 15.3 mV because of the decreased number of hydroxyl groups after the esterification reaction. In addition, CCP-Im exhibited a positive charge (42.1 mV), indicating the presence of imidazolium cations in the cellulose, which is beneficial for treating wastewater that contains anionic dyes.

Computer simulation

To study the interaction between the IM-IL structure of CCP-Im and dye molecules, Gaussian 09 was used to calculate the binding energy (ΔE) between the two compounds. To facilitate the simulations, the CCP-Im was simplified to Compound **1**, as shown in Fig. S1, and a similar method has been reported (Guan et al. 2015). In addition, three kinds of four different dye molecules (CR and XO (anionic dyes), MB (cationic dye), and DY (neutral dye)) were selected for this study. As shown in Fig. 5a, the value of ΔE between the cationic dye MB and Compound **1** could not be obtained because the electrostatic repulsion was higher than the bonding force. In contrast, the value of ΔE between the neutral dye DY and Compound **1** (Fig. 5b) was − 103.98 kJ mol^{-1}, and this might be because of hydrogen bonding and π–π stacking interactions. Finally, the binding energy between Compound **1** and XO as well as CR (Fig. 5c, d) were − 277.06 and − 143.52 kJ mol^{-1}, respectively, and these values indicate that the multiple interactions of
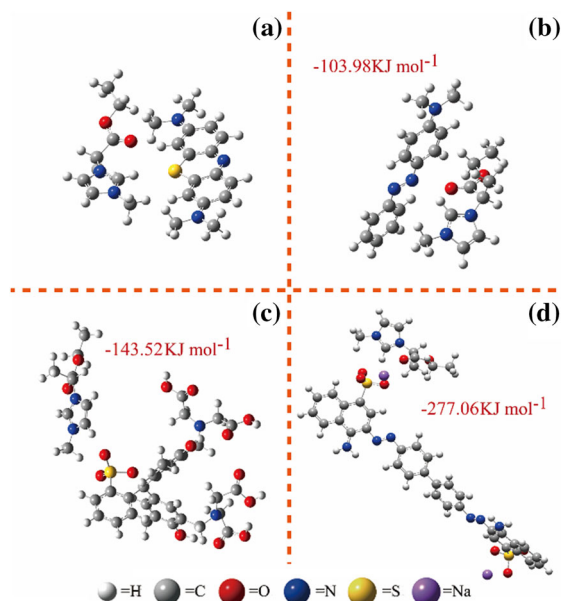
Fig. 5 Interactions between Compound **1** and **a** MB, **b** DY, **c** XO, and **d** CR

Compound **1** favor the adsorption performance of CCP-Im for anionic dye.

Optimization of adsorption conditions of CCP-Im

Effects of adsorbent dosage, pH, contact time, and initial concentration on adsorption capacities of the dyes were investigated in the adsorption experiments to optimize the adsorption conditions. As shown in Fig. S3, using the anionic dyes CR and XO as examples, the adsorption capacity changed slightly with pH in the range of 2–7. However, when pH was higher than 7, the adsorption capacity of CCP-Im dramatically decreased because excess OH^{-} ions compete with the dye anions for the adsorption sites.

In contrast, Fig. S4 shows that the impact of adsorbent dosage was inversely proportional to the adsorption capacity. This is because the quantity of dye adsorbed per unit weight of the adsorbent is reduced, causing a decrease in the utility of active sites utilization ratio (Li et al. 2011; Nandi et al. 2009).

As shown in Figs. S5 and S6, the adsorption capacity gradually increased with increases in the contact time and dye concentration under constant temperature. In addition, adsorption saturation was achieved when the concentrations of CR and XO were 2000 mg L^{-1} and the contact time was 24 h, as shown in Table S1. Using a similar experimental method, the optimal adsorption conditions for the neutral dye DY and the cationic dye MB were each determined, and the results are shown in Table S1.

Adsorption performance of CCP-Im

Adsorption experiments for both CCP and CCP-Im were carried out under the same conditions to verify the influence of the modification of IM-IL functional groups on the adsorption capacity of cellulose paper-based materials. In addition, the influence factor (IF) was obtained by dividing adsorption capacity of CCP-Im by CCP for quantitative comparison of the adsorption performances in this work.

As shown in Fig. 6, the value of IF for MB is only 0.9 because of electrostatic repulsions between the cationic imidazole group of CCP-Im and MB. Compared to MB, the IF of adsorption for DY is slightly higher, which might be a result of hydrogen bonding and π–π conjugate interactions between CCP-Im and
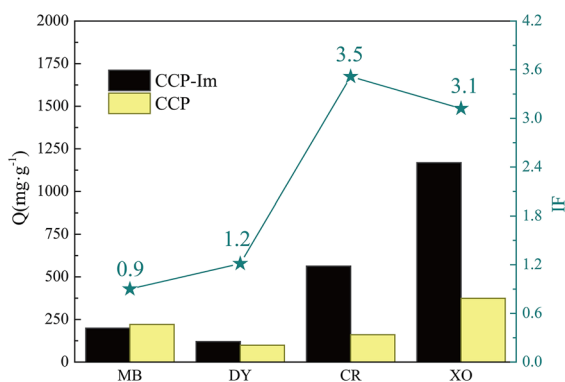
Fig. 6 Adsorption capacities and impact factors of CCP, CBE, and CCP-Im for various dyes under optimum adsorption conditions

DY. Unlike CCP-Im adsorption for MB and DY, the adsorption capacities of CCP-Im for XO and CR were significantly increased compared to that of CCP because of multiple interactions involving hydrogen bonding, π–π stacking, and electrostatic interactions. Also, the values of IF for XO and CR were 3.1 and 3.5, respectively. Consequently, the adsorption experimental results were in agreement with the trend in the theoretical values of binding energy between IM-IL functional groups and the dyes.

Adsorption mechanism of CCP-Im toward anionic dye

Adsorption kinetics Data for CR and XO (Fig. S5) were further analyzed and fitted using the two kinetics models (pseudo-first-order and pseudo-second-order) to study the adsorption rate of CCP-Im toward anionic dye (Xu et al. 2017; Wang et al. 2017). The pseudo-first-order Eq. 4 and pseudo-second-order Eq. 5 are expressed as follows:

$$\ln(q - q_t) = \ln q - t k_f \tag{4}$$

$$\frac{t}{q_t} = \frac{1}{k_s q^2} + \frac{t}{q} \tag{5}$$

where q_t (mg g^{-1}) and q (mg g^{-1}) are the calculated maximum adsorption capacity and experimental adsorption capacity, respectively, at time t (min); k_f (min^{-1}) and k_s (g mg^{-1} min^{-1}) are the rate constants of the pseudo-first-order and pseudo-second-order kinetics models, respectively. The pseudo-first-order model is commonly used to describe a physical adsorption process in which there is a linear relationship between the reaction rate and the concentration of a reactant (Eris and Azizian 2017). The pseudo-second-order model universally describes chemical sorption between an adsorbent and adsorbate (Bouabidi et al. 2018).

As shown in Fig. S7a, b and Table 1, the pseudo-second-order model fit both the CR and XO adsorption experiments better than the pseudo-first-order model because of the higher correlation coefficient (R^2). Moreover, as shown in Table 1, the calculated values of q were closer to the experimental Q values of both CR and XO, indicating that the actual adsorption processes of XO and CR were mainly controlled by the chemical adsorption mechanism.

Table 1 Parameters calculated from the adsorption kinetics models

Kinetic model	Parameter	CR	XO
Experimental value	Q (mg g^{-1})	563 ± 21	1169 ± 15
Pseudo-first-order	q_1 (mg g^{-1})	348.6	583.4
	k_f (min^{-1})	0.0051	0.0066
	R_1^2	0.914	0.742
Pseudo-second-order	q_2 (mg g^{-1})	574.7	1177.9
	k_s (10^{-5} g mg^{-1} min^{-1})	21.781	1.243
	R_2^2	0.990	0.9997
W-M model	$k_{\text{W-M},1}$ (mg g^{-1} min$^{-1/2}$)	34.187	129.213
	C_1	83.493	27.338
	$R_{\text{W-M},1}^2$	0.998	0.999
	$k_{\text{W-M},2}$ (mg g^{-1} min$^{-1/2}$)	12.146	7.848
	C_2	264.806	923.480
	$R_{\text{W-M},2}^2$	0.988	0.999

The W-M model (intraparticle diffusion model) was further employed to identify the factors that control the rates of the adsorption processes of CR and XO. The rate parameter of intraparticle diffusion can be defined as Eq. 6 as follows:

$$q = k_{\text{W-M}} t^{1/2} + C \tag{6}$$

where $k_{\text{W-M}}$ is the intraparticle diffusion rate constant, and C is related to the effect of the boundary layer on molecular diffusion. If the regression of q versus $t^{1/2}$ is linear and passes through the origin, then intraparticle diffusion is the only rate-limiting step (Álvarez-Gutiérrez et al. 2017; Azad et al. 2016).

As shown in Table 1, the high values of R^2 of both CR and XO revealed that the W-M model could be used to describe the adsorption process well. As shown in Fig. S7c, neither fitted line for CR nor XO passes through the origin, and this indicates that the adsorption rate was controlled by multiple stages in addition to internal diffusion. Besides, the fitted lines for CCP-Im can be separated into two linear regions, confirming that the adsorption processes can be divided into two parts: adsorption on the external surface stage and adsorption on the internal diffusion stage (Al Swat et al. 2017). The higher slope of the first region indicates that the rate of dye adsorption was faster in the first stage because of diffusion on the surface or in the macropores (Wang et al. 2013). The lower slope of the second subdued portion was caused by decreased concentration gradients, which prolonged diffusion of the dyes into the micropores of the adsorbent and

resulted in low adsorption rates (Foo and Hameed 2012).

Adsorption isotherms The Langmuir and Freundlich isotherm models were used to fit the adsorption data of XO and CR to further investigate the adsorption behavior of CCP-Im for anionic dyes (Liu et al. 2018a, b). The Langmuir Eq. 7 and Freundlich Eq. 8 are expressed as follows:

$$\frac{C}{q} = \frac{C}{q_m} + \frac{1}{K_L q_m} \tag{7}$$

$$\ln q = \ln K_F + \frac{1}{n} \ln C \tag{8}$$

where q_m is the calculated maximum adsorption capacity. K_L is the Langmuir constant related to binding affinity, and K_F is the Freundlich constant related to adsorption capacity. $1/n$ is the Freundlich constant related to adsorption intensity.

Usually, the Langmuir isotherm describes homogeneous adsorption, in which all of the sites have equal affinity for the adsorbate (Ghaedi et al. 2015). In addition, the Freundlich isotherm commonly assumes that the adsorption phenomena on heterogeneous adsorbent surfaces follow an empirical equation (Zhang et al. 2016a, b). As shown in Fig. S8 (a) and (b) and Table 2, the Freundlich model can better explain the adsorption isotherms for CR and XO because they have higher R^2 values than those of the Langmuir model. Thus, the results show that the adsorption of CCP-Im toward XO and CR occurred on a heterogeneous surface with nonuniform distribution

Table 2 Parameters calculated from the adsorption isotherms models

Isotherm model	Parameter	CR	XO
Langmiur	Q (mg g^{-1})	563 ± 21	1169 ± 15
	q_m (mg g^{-1})	598.8	1218.4
	K_L (L mg^{-1})	0.014	0.008
	R_L^2	0.845	0.886
Freundlich	K_F (mg g^{-1})	14.401	26.899
	$1/n$	0.600	0.565
	R_F^2	0.9998	0.9989
Scatchard	$q_{m,L}$ (mg g^{-1})	50.1	173.3
	$K_{S,L}$ (L mg^{-1})	1.173	7.343
	$R_{S,L}^2$	0.952	0.952
	$q_{m,H}$ (mg g^{-1})	710.5	1361.7
	$K_{S,H}$ (L mg^{-1})	162.338	240.964
	$R_{S,H}^2$	0.909	0.904

$K_{S,H}$ and $K_{S,L}$ are the adsorption equilibrium constants for 'high-affinity' and 'low-affinity' binding sites, respectively

of adsorption heat and affinities (Foo and Hameed 2012). Furthermore, the $1/n$ values of both CR and XO were less than 1, suggesting that there are favorable adsorption behaviors for these anionic dyes on CCP-Im (Qian et al. 2015; Mashtalir et al. 2014).

To further study the adsorption behavior of CCP-Im, the data for CR and XO were analyzed using the Scatchard model (Yu et al. 2017). The Scatchard equation is as follows:

$$\frac{q}{C} = \frac{q_m}{K_S} - \frac{q}{K_S} \tag{9}$$

where q_m and K_S are the Scatchard constants related to the theoretical maximum adsorption capacity and the binding affinity, respectively.

Because of sensitivity to the heterogeneous and cooperative binding effect, Scatchard analysis was used to estimate the binding properties, such as the types of binding sites and the corresponding binding affinities between adsorbent and adsorbate (Liu and Chen 2015). Generally, if a fitting result shows a linear plot, it indicates that there is one kind of identical and independent binding site. However, if there is a deviation from linearity in a Scatchard fitting plot (two inflections), it indicates the presence of more than one type of binding site contributing to the adsorption (Zhang et al. 2016a, b).

As shown in Fig. S8c and Table 2, neither the Scatchard model fitting curve of CR nor XO for CCP-Im is a single straight line, and this further confirms that the binding sites of CCP-Im were heterogeneous in the adsorption process. In addition, the two sections of the fitted curves that have different slopes for both CR and XO indicate that CCP-Im has two types of adsorption binding sites for anionic dyes: high-affinity and low-affinity binding sites (Gong et al. 2017). This conclusion is also consistent with the fitted results of the Freundlich model.

Adsorption thermodynamics Thermodynamics analysis of an adsorption process provides information on spontaneity. Adsorption experiments were carried out with temperature as a variable to study the thermodynamics. The effects of temperature on the adsorption capacity of CCP-Im are shown in Fig. S9 (Fayoud et al. 2015). The adsorption capacities of XO and CR are reduced by 38.32 and 35.06 mg g^{-1}, respectively, after the temperature was increased by 60 K. Because the adsorption capacity decreased with an increase in temperature, it is determined that CCP-Im adsorption on anionic dye is an exothermic process (Luo et al. 2017).

Changes in the standard Gibbs energy (ΔG), enthalpy (ΔH), and entropy (ΔS) for the dyes CR and XO were calculated from experimental data obtained at different temperatures. The curves obtained from plotting ln (Q/C_e) against $1/T$ based on Eq. 10 are shown in Fig. S10. Also the value of the parameter ΔG at a certain temperature was calculated using Eq. 11, and the calculated results are listed in Table 3.

$$\ln \frac{Q}{Ce} = -\frac{\Delta H}{RT} + \frac{\Delta S}{R} \tag{10}$$

$$\Delta G = -RT \ln \frac{Q}{Ce} \tag{11}$$

As shown in Table 3, all of the ΔG values were negative, indicating the spontaneous nature of the dye adsorption on CCP-Im. The value of ΔG for the adsorption process became less negative as the temperature increased, and this was probably because the strong interactions between CCP-Im and anionic dyes decrease substantially with an increase in temperature (Kang et al. 2017). In addition, the negative values of ΔH indicate the exothermic nature of the adsorption process, which is in agreement with

Table 3 Parameters calculated from adsorption thermodynamics models

| Dye	R^2	ΔH (KJ mol^{-1})	ΔS (J mol^{-1} K^{-1})	ΔG (KJ mol^{-1}) at different temperatures			
				293.15 K	313.15 K	333.15 K	353.15 K
CR	0.996	− 2.02	− 4.79	− 0.62	− 0.53	− 0.43	− 0.34
XO	0.998	− 1.12	− 0.99	− 0.83	− 0.81	− 0.79	− 0.77

R^2 is the correlation coefficient. R is the universal gas constant (8.315 J/mol K)

experimental results that show that lower temperature leads to higher adsorption capacity.

Selective adsorption of CR from mixture solution

Industrial wastewater composition contains various types of dyes, which may compete for the adsorption sites of CCP-Im and thus decrease the adsorption efficiency (Zhang et al. 2014). In this work, selective adsorption experiments were carried out to further verify the adsorption performance of CCP-Im for anionic dyes of binary solution systems.

As shown in Fig. 7, in the UV absorption curve for the mixture solution after adsorption, the peak intensity decreased significantly at 497 nm after a contact time of 24 h, whereas the peak intensity at 667 nm remained almost unchanged. It was concluded that CR could be almost completely removed from the mixture solution after the adsorption by CCP-Im, indicating that CCP-Im can be used for selective adsorption of anionic dyes from mixed solutions.
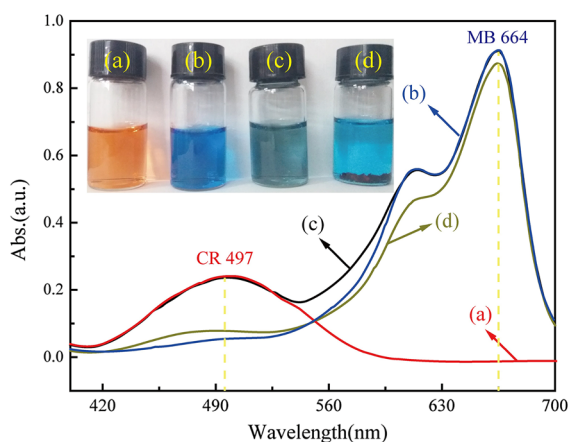
Fig. 7 UV–Vis spectra of aqueous solutions of CR (**a**), MB (**b**), CR + MB mixture (**c**) and CR + MB after the addition of CCP-Im (**d**) (C$_{0, \text{dyes}}$ = 5 mg L^{-1}, V$_{\text{dye}}$ = 6 mL, m$_{\text{adsorbent}}$ = 30 mg, pH = 7, t = 24 h, T = 293.15 K)

Recycling studies-successive adsorption–desorption cycles

Reusability is an important criterion for a material to be applicable for practical purposes. Five consecutive adsorption–desorption cycles were performed to evaluate the stability and reusability of CCP-Im upon recycling. As shown in Table S2, after five cycles of adsorption–desorption, the Q_n/Q_0 value of CCP-Im still remained 82.13%, suggesting that CCP-Im can be used cyclically. This important feature demonstrates that CCP-Im can be effectively regenerated and reused for sustainable treatment of dyes in wastewater.

Conclusions

In summary, a cellulose-based bioadsorbent was designed and prepared by grafting IM-IL functional groups onto cellulose paper. Compared to the original cellulose material CCP, CCP-Im exhibited excellent adsorption performance because of the strong multiple interactions between the imidazole structure and dye molecules, and thus, CCP-Im can be used to address the complex issue of treating anionic dyes in wastewater. Therefore, developing this low cost, eco-friendly, and efficient bioadsorbent is a promising way to resolve the environmental issues involved in sustainable development.

References

Al Swat AA, Saleh TA, Ganiyu SA, Siddiqui MN, Alhooshani KR (2017) Preparation of activated carbon, zinc oxide and nickel oxide composites for potential application in the desulfurization of model diesel fuels. J Anal Appl Pyrol 128:246–256. https://doi.org/10.1016/j.jaap.2017.10.004

Álvarez-Gutiérrez N, Gil MV, Rubiera F, Pevida C (2017) Kinetics of CO_2 adsorption on cherry stone-based carbons in CO_2/CH_4 separations. Chem Eng J 307:249–257. https://doi.org/10.1016/j.cej.2016.08.077

Azad FN et al (2016) Optimization of the process parameters for the adsorption of ternary dyes by Ni doped FeO(OH)-NWs–AC using response surface methodology and an artificial neural network. RSC Adv 6:19768–19779. https://doi.org/10.1039/c5ra26036a

Boakye FO, Fan ML, Cai HP, Zhang HN (2017) Nitrogen-doped porous carbon derived from imidazole-functionalized polyhedral oligomeric silsesquioxane. J Mater Sci 53:456–465. https://doi.org/10.1007/s10853-017-1522-7

Bouabidi ZB, El-Naas MH, Cortes D, McKay G (2018) Steel-making dust as a potential adsorbent for the removal of lead (II) from an aqueous solution. Chem Eng J 334:837–844. https://doi.org/10.1016/j.cej.2017.10.073

Buthiyappan A, Abdul Raman AA, Daud WMAW (2016) Development of an advanced chemical oxidation wastewater treatment system for the batik industry in Malaysia. RSC Adv 6:25222–25241. https://doi.org/10.1039/c5ra26775g

Chen X, Zheng N, Wang Q, Liu LZ, Men YF (2017) Side-chain crystallization in alkyl-substituted cellulose esters and hydroxypropyl cellulose esters. Carbohyd Polym 162:28–34. https://doi.org/10.1016/j.carbpol.2017.01.028

Eris S, Azizian S (2017) Extension of classical adsorption rate equations using mass of adsorbent: a graphical analysis. Sep Purif Technol 179:304–308. https://doi.org/10.1016/j.seppur.2017.02.021

Fayoud N, Tahiri S, Alami Younssi S, Albizane A, Gallart-Mateu D, Cervera ML, de la Guardia M (2015) Kinetic, isotherm and thermodynamic studies of the adsorption of methylene blue dye onto agro-based cellulosic materials. Desalination Water Treat 57:16611–16625. https://doi.org/10.1080/19443994.2015.1079249

Foo KY, Hameed BH (2012) Coconut husk derived activated carbon via microwave induced activation: effects of activation agents, preparation parameters and adsorption performance. Chem Eng J 184:57–65. https://doi.org/10.1016/j.cej.2011.12.084

Fu J et al (2016) Selective adsorption and separation of organic dyes from aqueous solution on polydopamine microspheres. J Colloid Interface Sci 461:292–304. https://doi.org/10.1016/j.jcis.2015.09.017

Ghaedi M, Hajjati S, Mahmudi Z, Tyagi I, Agarwal S, Maity A, Gupta VK (2015) Modeling of competitive ultrasonic assisted removal of the dyes—methylene blue and safranin-O using Fe_3O_4 nanoparticles. Chem Eng J 268:28–37. https://doi.org/10.1016/j.cej.2014.12.090

Góes MM, Keller M, Masiero Oliveira V, Villalobos LDG, Moraes JCG, Carvalho GM (2016) Polyurethane foams synthesized from cellulose-based wastes: kinetics studies

of dye adsorption. Ind Crops Prod 85:149–158. https://doi.org/10.1016/j.indcrop.2016.02.051

Gong C et al (2017) A molecular imprinting-based multifunctional chemosensor for phthalate esters. Dyes Pigm 137:499–506. https://doi.org/10.1016/j.dyepig.2016.10.047

Guan G et al (2015) Protein Induces layer-by-layer exfoliation of transition metal dichalcogenides. J Am Chem Soc 137:6152–6155. https://doi.org/10.1021/jacs.5b02780

Han G, Liang CZ, Chung TS, Weber M, Staudt C, Maletzko C (2016) Combination of forward osmosis (FO) process with coagulation/flocculation (CF) for potential treatment of textile wastewater. Water Res 91:361–370. https://doi.org/10.1016/j.watres.2016.01.031

He YC, Yang J, Kan WQ, Zhang HM, Liu YY, Ma JF (2015) A new microporous anionic metal-organic framework as a platform for highly selective adsorption and separation of organic dyes. J Mater Chem A 3:1675–1681. https://doi.org/10.1039/c4ta05391e

Hokkanen S, Bhatnagar A, Sillanpaa M (2016) A review on modification methods to cellulose-based adsorbents to improve adsorption capacity. Water Res 91:156–173. https://doi.org/10.1016/j.watres.2016.01.008

Kang W et al (2017) A pH-responsive wormlike micellar system of a noncovalent interaction-based surfactant with a tunable molecular structure. Soft Matter 13:1182–1189. https://doi.org/10.1039/c6sm02655a

Karatzos SK, Edye LA, Wellard RM (2011) The undesirable acetylation of cellulose by the acetate ion of 1-ethyl-3-methylimidazolium acetate. Cellulose 19:307–312. https://doi.org/10.1007/s10570-011-9621-0

Li WH, Yue QY, Gao BY, Ma ZH, Li YJ, Zhao HX (2011) Preparation and utilization of sludge-based activated carbon for the adsorption of dyes from aqueous solutions. Chem Eng J 171:320–327. https://doi.org/10.1016/j.cej.2011.04.012

Li B, Dong Y, Li L (2015) Preparation and catalytic performance of Fe(III)-citric acid-modified cotton fiber complex as a novel cellulose fiber-supported heterogeneous photo—Fenton catalyst. Cellulose 22:1295–1309. https://doi.org/10.1007/s10570-015-0562-x

Lin J et al (2016) Tight ultrafiltration membranes for enhanced separation of dyes and Na_2SO_4 during textile wastewater treatment. J Membr Sci 514:217–228. https://doi.org/10.1016/j.memsci.2016.04.057

Liu H, Chen W (2015) Magnetic mesoporous imprinted adsorbent based on Fe_3O_4-modified sepiolite for organic micropollutant removal from aqueous solution. RSC Adv 5:27034–27042. https://doi.org/10.1039/c5ra00985e

Liu K, Chen L, Huang L, Lai Y (2016) Evaluation of ethylenediamine-modified nanofibrillated cellulose/chitosan composites on adsorption of cationic and anionic dyes from aqueous solution. Carbohyd Polym 151:1115–1119. https://doi.org/10.1016/j.carbpol.2016.06.071

Liu X, Jia J, Rueping M (2017) Nickel-catalyzed C–O bond-cleaving alkylation of esters: direct replacement of the ester moiety by functionalized alkyl chains. ACS Catal 7:4491–4496. https://doi.org/10.1021/acscatal.7b00941

Liu Q et al (2018a) A facile route to the production of polymeric nanofibrous aerogels for environmentally sustainable

applications. J Mater Chem A 6:3692–3704. https://doi.org/10.1039/C7TA10107D

Liu J, Wang Z, Li H, Hu C, Raymer P, Huang Q (2018b) Effect of solid state fermentation of peanut shell on its dye adsorption performance. Biores Technol 249:307–314. https://doi.org/10.1016/j.biortech.2017.10.010

Luo L, Jin Y, Li M, Hu L, Li J, Liu Y (2017) Adsorption mechanism of anionic groups found in sulfonated mulberry stem chemi-mechanical pulp (SCMP) for removal of methylene blue dye. BioResources 12:2452–2465. https://doi.org/10.15376/biores.12.2.2452-2465

Maneerung T, Liew J, Dai Y, Kawi S, Chong C, Wang CH (2016) Activated carbon derived from carbon residue from biomass gasification and its application for dye adsorption: kinetics, isotherms and thermodynamic studies. Biores Technol 200:350–359. https://doi.org/10.1016/j.biortech.2015.10.047

Mashtalir O, Cook KM, Mochalin VN, Crowe M, Barsoum MW, Gogotsi Y (2014) Dye adsorption and decomposition on two-dimensional titanium carbide in aqueous media. J Mater Chem A 2:14334–14338. https://doi.org/10.1039/c4ta02638a

Melo BC, Paulino FAA, Cardoso VA, Pereira AGB, Fajardo AR, Rodrigues FHA (2018) Cellulose nanowhiskers improve the methylene blue adsorption capacity of chitosan-g-poly (acrylic acid) hydrogel. Carbohyd Polym 181:358–367. https://doi.org/10.1016/j.carbpol.2017.10.079

Mi H, Jiang Z, Kong J (2013) Hydrophobic poly (ionic liquid) for highly effective separation of methyl blue and chromium ions from water. Polymers 5:1203–1214. https://doi.org/10.3390/polym5041203

Mir AA, Amooey AA, Ghasemi S (2018) Adsorption of direct yellow 12 from aqueous solutions by an iron oxide-gelatin nanoadsorbent; kinetic, isotherm and mechanism analysis. J Clean Prod 170:570–580. https://doi.org/10.1016/j.jclepro.2017.09.101

Nandi BK, Goswami A, Purkait MK (2009) Adsorption characteristics of brilliant green dye on kaolin. J Hazard Mater 161:387–395. https://doi.org/10.1016/j.jhazmat.2008.03.110

Peng X, Hu F, Zhang T, Qiu F, Dai H (2018) Amine-functionalized magnetic bamboo-based activated carbon adsorptive removal of ciprofloxacin and norfloxacin: a batch and fixed-bed column study. Biores Technol 249:924–934. https://doi.org/10.1016/j.biortech.2017.10.095

Qian L et al (2015) The effectively specific recognition of bovine serum albumin imprinted silica nanoparticles by utilizing a macromolecularly functional monomer to stabilize and imprint template. Anal Chim Acta 884:97–105. https://doi.org/10.1016/j.aca.2015.05.015

Qian L et al (2017) Immobilization of BSA on ionic liquid functionalized magnetic Fe_3O_4 nanoparticles for use in surface imprinting strategy. Talanta 168:174–182. https://doi.org/10.1016/j.talanta.2017.03.044

Qiu Y, Zheng Z, Zhou Z, Sheng GD (2009) Effectiveness and mechanisms of dye adsorption on a straw-based biochar. Biores Technol 100:5348–5351. https://doi.org/10.1016/j.biortech.2009.05.054

Song W et al (2016) Hyperbranched polymeric ionic liquid with imidazolium backbones for highly efficient removal of anionic dyes. Chem Eng J 287:482–491. https://doi.org/10.1016/j.cej.2015.11.039

Song K, Xu H, Xu L, Xie K, Yang Y (2017) Cellulose nanocrystal-reinforced keratin bioadsorbent for effective removal of dyes from aqueous solution. Biores Technol 232:254–262. https://doi.org/10.1016/j.biortech.2017.01.070

Trache D, Hussin MH, Haafiz MKM, Thakur VK (2017) Recent progress in cellulose nanocrystals: sources and production. Nanoscale 9:1763–1786. https://doi.org/10.1039/c6nr09494e

Umukoro EH, Peleyeju MG, Ngila JC, Arotiba OA (2017) Towards wastewater treatment: photo-assisted electrochemical degradation of 2-nitrophenol and orange II dye at a tungsten trioxide-exfoliated graphite composite electrode. Chem Eng J 317:290–301. https://doi.org/10.1016/j.cej.2017.02.084

Veerakumar P, Tharini J, Ramakrishnan M, Panneer Muthuselvam I, Lin KC (2017) Graphene oxide nanosheets as an efficient and reusable sorbents for eosin yellow dye removal from aqueous solutions. ChemistrySelect 2:3598–3607. https://doi.org/10.1002/slct.201700281

Wang C, Zhang J, Wang P, Wang H, Yan H (2013) Adsorption of methylene blue and methyl violet by camellia seed powder: kinetic and thermodynamic studies. Desalination Water Treat 53:3681–3690. https://doi.org/10.1080/19443994.2013.873881

Wang F, Pan Y, Cai P, Guo T, Xiao H (2017) Single and binary adsorption of heavy metal ions from aqueous solutions using sugarcane cellulose-based adsorbent. Biores Technol 241:482–490. https://doi.org/10.1016/j.biortech.2017.05.162

Watson BL, Moore TA, Moore AL, Gust D (2017) Synthesis of a novel building block for the preparation of multi-chromophoric sensitizers for panchromatic dye-sensitized solar cells. Dyes Pigm 136:893–897. https://doi.org/10.1016/j.dyepig.2016.09.037

Xiao J, Lv W, Xie Z, Tan Y, Song Y, Zheng Q (2016) Environmentally friendly reduced graphene oxide as a broad-spectrum adsorbent for anionic and cationic dyes via π–π interactions. J Mater Chem A 4:12126–12135. https://doi.org/10.1039/c6ta04119a

Xu Q, Wang Y, Jin L, Wang Y, Qin M (2017) Adsorption of Cu (II), Pb(II) and Cr(VI) from aqueous solutions using black wattle tannin-immobilized nanocellulose. J Hazard Mater 339:91–99. https://doi.org/10.1016/j.jhazmat.2017.06.005

Yao S et al (2017) An anionic metal-organic framework with ternary building units for rapid and selective adsorption of dyes. Dalton Trans 46:3332–3337. https://doi.org/10.1039/C7DT00192D

Yu Z et al (2017) Preparation and characterization of poly (maleic acid)-grafted cross-linked chitosan microspheres for Cd(II) adsorption. Carbohyd Polym 172:28–39. https://doi.org/10.1016/j.carbpol.2017.05.039

Zhang P, Yin J, Jiang X (2014) Hyperbranched poly (ether amine) (hPEA)/poly (vinyl alcohol) (PVA) interpenetrating network (IPN) for selective adsorption and separation of guest homologues. Langmuir 30:14597–14605. https://doi.org/10.1021/la502869n

Zhang Y, Xie Z, Teng X, Fan J (2016a) Synthesis of molecularly imprinted polymer nanoparticles for the fast and highly

selective adsorption of sunset yellow. J Sep Sci 39:1559–1566. https://doi.org/10.1002/jssc.201501295

Zhang H et al (2016b) Removal of methyl orange from aqueous solutions by adsorption on cellulose hydrogel assisted with Fe_2O_3 nanoparticles. Cellulose 24:903–914. https://doi.org/10.1007/s10570-016-1129-1

Zhu W et al (2016) Functionalization of cellulose with hyperbranched polyethylenimine for selective dye adsorption and separation. Cellulose 23:3785–3797. https://doi.org/10.1007/s10570-016-1045-4